


Impurity-induced resonant states in topological nodal-line semimetalsTao Zhou^{1,2,*}, Wei Chen,^{3,4} Yi Gao,⁵ and Z. D. Wang^{2,†}¹*Guangdong Provincial Key Laboratory of Quantum Engineering and Quantum Materials, GPETR Center for Quantum Precision Measurement, SPTE, South China Normal University, Guangzhou 510006, China*²*Department of Physics and Center of Theoretical and Computational Physics, The University of Hong Kong, Pokfulam Road, Hong Kong, China*³*Institute for Theoretical Physics, ETH Zurich, 8093 Zürich, Switzerland*⁴*College of Science, Nanjing University of Aeronautics and Astronautics, Nanjing 210016, China*⁵*Department of Physics and Institute of Theoretical Physics, Nanjing Normal University, Nanjing, 210023, China* (Received 27 May 2019; revised manuscript received 22 October 2019; published 12 November 2019)

Nodal-line semimetals are characterized by a kind of topologically nontrivial bulk-band crossing, giving rise to almost flat surface states. Notably, direct evidence of the surface states is still awaited. Here we theoretically study impurity effects in topological nodal-line semimetals based on the T -matrix method. It is found that some low energy states may be induced near the impurity site for a bulk impurity, while the visible resonant impurity state can only exist for certain impurity strength. For a surface impurity, a robust resonant impurity state exists in a wide parametric range of impurity strength. Such robust resonant state stems from the topologically protected weak dispersive surface states, which can be probed by scanning tunneling microscopy, providing a clear signature of the topological surface states in the nodal-line semimetals.

DOI: [10.1103/PhysRevB.100.205119](https://doi.org/10.1103/PhysRevB.100.205119)**I. INTRODUCTION**

Three-dimensional topological nodal-line semimetals (NLSs) have recently attracted a great interest in condensed matter physics and materials science [1–38]. These NLSs are generally characterized by band-crossing closed loops near the Fermi level. Each loop carries a π Berry flux, leading to the nontrivial surface states. The bulk and surface states may be responsible for a number of interesting and important properties as well as potential applications, such as unique symmetric behaviors [4], surface Chern insulators [5], nontrivial transport properties [6–11], giant Friedel oscillations [12], long-range Coulomb interactions [13,14], and a possible route to high- T_c superconductivity [15].

Recently, the NLS has been proposed theoretically or reported experimentally in various systems, including the Cu_3XN family ($X = \text{Ni, Cu, Pd, Ag, Cd}$) [2,3], alkaline-earth metals [12,16], group-IV tellurides (SnTe, GeTe) [17], the WX_3 family ($W = \text{Gd, Zr, Hf, La; H = Si, Ge, Sn, Sb; X = O, S, Se, Te}$) [6–9,18–23], the XTaSe_2 family ($X = \text{Pb, Tl}$) [24,25], the CaTX family ($T = \text{Cd, Ag; X = P, Ge, As}$), the YX_3 family ($Y = \text{Ca, Sr, Ba; X = P, AS}$) [26,27], PtSn_4 [28], Ta_3SiTe_6 [29], AlB_2 [30], Ca_3P_2 [31,32], and the cold atom system [33,34]. The research progress on the NLSs has made it possible to study further physical properties of these systems. On the other hand, so far more evidence to hallmark the NLSs, especially the surface states therein, are still awaited.

The single impurity effect is an important tool for understanding quantum states in various solid-state systems [39], which is rather powerful especially for the gapped systems. The in-gap bound states may be induced by an impurity, through which some hidden properties may be detected. Theoretically, the impurity-induced bound states are manifested in the local density of states (LDOS) near the impurity site [39]. Experimentally, they can be measured through scanning tunneling microscopy (STM) [40]. Previously, the single impurity effects have been widely used to investigate physical properties, such as the pairing symmetry in various unconventional superconductors [39,41–43]. They have also been studied intensively in various topologically nontrivial systems, including several topological superconductor/superfluid systems [44–52], topological insulators [53–55], and topological Weyl semimetals [56]. The NLS is a relatively new one to a family of topological materials. Previously the quasiparticle interference in the normal and superconducting NLSs was studied theoretically [52]. The possible resonant state of the NLSs with the d -wave superconducting order was also discussed [52], while to the best of our knowledge, it is still awaited for us to theoretically study the single impurity effects in the normal state of NLSs, which may provide an effective way to detect the unique properties of the NLS.

In this paper, we study theoretically the single impurity effects based on the T -matrix method [57,58] with different impurity strengths starting from an effective model to describe the NLS system. Given that the bulk and surface states in the NLSs possess completely different properties, it can be expected that the impurity effects in the bulk and surface states should also lead to different results. The LDOS spectra near a bulk and surface impurity site are studied. For a bulk impurity, some low-energy states may be induced, while the resonant

*tzhou@scnu.edu.cn

†zwang@hku.hk

impurity state can only exist for a typical impurity strength. In contrast, a resonant bound state induced by the surface impurity is revealed for a rather wide parametric range of impurity strengths. This bound state is due to the topologically protected quasiflat band at the system surface. We compare the results with that in the Weyl semimetal and show that the exotic surface states of the NLS can be detected through the surface impurity effects.

The rest of our paper is organized as follows. In Sec. II, we introduce the model and present the relevant formalism. In Sec. III, we report numerical calculations and discuss the obtained results. Finally, we give a brief summary in Sec. IV.

II. MODEL AND FORMALISM

The NLS may contain one or more nodal lines with various configurations. For the latter case with nodal lines well separated in the reciprocal space, we assume that the impurity-induced scattering between different nodal lines is negligibly small. Therefore, it is sufficient to consider the NLS carrying one nodal loop, which can be captured by the Hamiltonian on a cubic lattice as

$$H = \sum_{\mathbf{k}} \varepsilon(\mathbf{k})\sigma_0 + \sum_{\mathbf{k}} M(\mathbf{k})\sigma_3 + \sum_{\mathbf{k}} \lambda(\mathbf{k})\sigma_2, \quad (1)$$

where σ_0 is the 2×2 identity matrix and $\sigma_{2,3}$ are Pauli matrices in the two-band space. $\varepsilon(\mathbf{k}) = -2 \sum_{\alpha=x,y,z} t_{0\alpha} \cos k_\alpha - \mu$, $M(\mathbf{k}) = -2 \sum_{\alpha=x,y,z} t_{1\alpha} \cos k_\alpha - h$, and $\lambda(\mathbf{k}) = 2\lambda_0 \sin k_y$. Then we obtain two energy bands from the above Hamiltonian as $E_{\pm}(\mathbf{k}) = \varepsilon(\mathbf{k}) \pm \sqrt{M(\mathbf{k})^2 + \lambda(\mathbf{k})^2}$. The first term breaks the chiral symmetry ($[H, \sigma_1]_+ = 0$) of the system and thus introduces finite dispersion to the surface states [1]. Nevertheless, it will not change the band topology of the bulk states.

A point impurity term is given by

$$H_{\text{imp}} = V_s \sum_{\sigma} c_{\mathbf{r}_0\sigma}^{\dagger} c_{\mathbf{r}_0\sigma}, \quad (2)$$

where V_s is the impurity strength. \mathbf{r}_0 is the site where the impurity locates. σ represents the spin or the pseudospin.

To study the effects of the surface impurity, let us consider a sample with finite thickness in the y direction with $1 \leq y \leq N_y$ (N_y is the number of lattice sites in the y direction) while the periodic boundary condition still holds in the x and z directions. Then the Hamiltonian is reduced to a quasi-two-dimensional one in the x - z plane by a partial Fourier transformation along the y direction as

$$\begin{aligned} H = & \sum_{\mathbf{k}, y, \sigma} \zeta_{\mathbf{k}\sigma} c_{y\sigma}^{\dagger}(\mathbf{k}) c_{y\sigma}(\mathbf{k}) \\ & - (\sigma t_{1y} + t_{0y}) \sum_{\mathbf{k}, y, \sigma} [c_{y\sigma}^{\dagger}(\mathbf{k}) c_{y+1, \sigma}(\mathbf{k}) + \text{H.c.}] \\ & + \sum_{\mathbf{k}, y} \left[\frac{\lambda}{2} c_{y\uparrow}^{\dagger}(\mathbf{k}) c_{y+1\downarrow}(\mathbf{k}) - \frac{\lambda}{2} c_{y\downarrow}^{\dagger}(\mathbf{k}) c_{y+1\uparrow}(\mathbf{k}) + \text{H.c.} \right], \end{aligned} \quad (3)$$

with the corresponding momentum being reduced to a two-dimensional one as $\mathbf{k} = \mathbf{k}_{\parallel} = (k_x, k_z)$ and $\zeta_{\mathbf{k}\sigma} = \sigma h - \mu - 2 \sum_{\alpha=x,z} (\sigma t_{1\alpha} + t_{0\alpha}) \cos k_\alpha$.

The Hamiltonian in Eqs. (1) and (3) can be written as the 2×2 and $2N_y \times 2N_y$ matrix $[H = \sum_{\mathbf{k}} \Psi^{\dagger}(\mathbf{k}) \hat{M} \Psi(\mathbf{k})]$, with $\Psi(\mathbf{k}) = (c_{\mathbf{k}\uparrow}, c_{\mathbf{k}\downarrow})^T$ and $\Psi(\mathbf{k}) = (c_{1\uparrow}(\mathbf{k}), c_{1\downarrow}(\mathbf{k}), \dots, c_{N_y\uparrow}(\mathbf{k}), c_{N_y\downarrow}(\mathbf{k}))^T$, respectively. In the following, we investigate the effects of both the bulk and surface impurities, in which periodic and open boundary conditions are adopted, respectively.

The bare Green's function matrix in the momentum space $\hat{G}_0(\mathbf{k}, \omega)$ can be obtained by diagonalizing the Hamiltonian, with the matrix elements being expressed as

$$G_{0ij}(\mathbf{k}, \omega) = \sum_n \frac{u_{i,n}(\mathbf{k}) u_{j,n}^*(\mathbf{k})}{\omega - E^n(\mathbf{k}) + i\Gamma}, \quad (4)$$

where u_{in} and E^n are the eigenvectors and eigenvalues of the Hamiltonian matrix H , respectively.

Following the standard technique of the T -matrix method [39], the T matrix and the full Green's function are expressed as

$$\hat{T}(\omega) = [\hat{I} - \hat{U} \hat{G}_0(\omega)]^{-1} \hat{U} \quad (5)$$

and

$$\hat{G}(\mathbf{r}, \mathbf{r}', \omega) = \hat{G}_0(\mathbf{r}, \mathbf{r}', \omega) + \hat{G}_0(\mathbf{r}, 0, \omega) \hat{T}(\omega) \hat{G}_0(0, \mathbf{r}', \omega). \quad (6)$$

Here, $\hat{G}_0(\mathbf{r}, \mathbf{r}', \omega) = \frac{1}{N} \sum_{\mathbf{k}} \hat{G}_0(\mathbf{k}, \omega) e^{i\mathbf{k} \cdot (\mathbf{r} - \mathbf{r}')}$ is the Fourier transformation of $\hat{G}_0(\mathbf{k}, \omega)$ and \hat{I} is the identity matrix. For a bulk impurity, \hat{U} is a 2×2 matrix with $\hat{U} = V_s \hat{I}$. For a surface impurity at the $y = 1$ plane, U is a $2N_y \times 2N_y$ matrix with two nonvanishing matrix elements $U_{11} = U_{22} = V_s$.

The LDOS can be calculated through

$$\rho(\mathbf{r}, \omega) = -\frac{1}{\pi} \text{Im}[G_{11}(\mathbf{r}, \mathbf{r}, \omega) + G_{22}(\mathbf{r}, \mathbf{r}, \omega)]. \quad (7)$$

In the present work, we set the parameters to $t_{1\alpha} = 1$, $\lambda = 0.5$, and $h = -4$. The band degeneracy points define a nodal line

$$\cos k_x + \cos k_z = 1; \quad k_y = 0. \quad (8)$$

In the presence of the spin (or pseudospin) independent hopping term with $\varepsilon(\mathbf{k}) \neq 0$, the surface states are dispersive [1]. In the following calculation, we set $t_{0x} = t_{0z} = 0.2$, $t_{0y} = 0.1$, and $\mu = -0.6$. Here, the chemical potential makes sure that the nodal line appears at the zero energy.

III. RESULTS AND DISCUSSIONS

We first study the topological band structure considering the periodic boundary condition along the x - z plane and the open boundary condition along the y direction with $1 \leq y \leq 200$. The eigenvalues through diagonalizing Hamiltonian of Eq. (3) as a function of k_z with $k_x = 0$ are plotted in Fig. 1. As $\varepsilon(\mathbf{k})$ equals to zero, the energy spectrum is symmetric about zero energy due to the chiral symmetry. A flat surface band appears at the Fermi energy, as seen in Fig. 1(a). The existence of the flat surface band can be well understood through treating the in-plane momentum \mathbf{k}_{\parallel} as effective parameters and the system reduces to be one-dimensional. One can define a topological invariant depending on \mathbf{k}_{\parallel} to illustrate

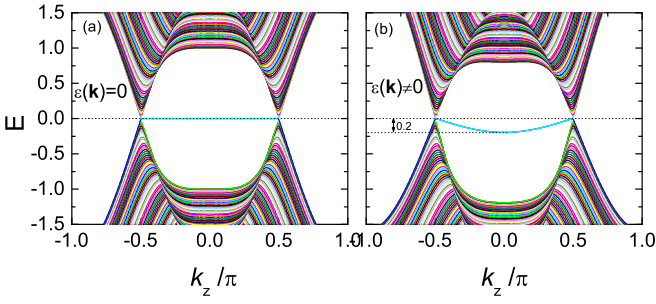


FIG. 1. The energy spectrum along the $k_x = 0$ cut with considering the open boundary condition along the y direction and the periodic boundary condition along the x and z directions.

the topological properties [4],

$$C(\mathbf{k}_{\parallel}) = -\frac{i}{\pi} \int_{-\pi}^{\pi} \langle u_n(\mathbf{k}) | \partial k_y | u_n(\mathbf{k}) \rangle dk_y, \quad (9)$$

where $u_n(\mathbf{k})$ is the eigenvector of the valence band. Then, we have $C = 1$ when the in-plane momentum \mathbf{k}_{\parallel} is inside the projection of the nodal loop, and $C = 0$ when \mathbf{k}_{\parallel} is elsewhere [cf. Fig. 1(a)]. Therefore, when \mathbf{k}_{\parallel} is inside the Fermi surface, there must be topologically protected boundary states if the open boundary along the y direction is considered. Without the chiral-symmetry-breaking term, the energy of boundary modes does not vary with \mathbf{k}_{\parallel} , leading to a flat band. In real materials of NLSs, there may exist a finite $\varepsilon(\mathbf{k})$ term. The energy spectrum in this case is plotted in Fig. 1(b). As is seen, for this case, the chiral symmetry is broken and the surface band has a dispersion with the bandwidth about 0.2 corresponding to the strength of t_{0x} and t_{0z} .

We now discuss the impurity effects of NLSs. We first present the numerical results with $\varepsilon(\mathbf{k}) = 0$. Two types of the point impurity will be considered here. One is the bulk impurity inside a three-dimensional sample with the periodic boundary condition in all of the three directions. A point impurity at the site $\mathbf{r} = (0, 0, 0)$ is considered. The other is an impurity at the site $\mathbf{r}_{\parallel} = (0, 0)$ on the open surface ($y = 1$) of the sample where the periodic boundary condition holds only in the x and z directions. In the calculation, the Hamiltonian in Eqs. (1) and (3) is adopted for the two cases, respectively. The LDOS spectra near a bulk impurity site [at the site (0,1,0)] with different impurity strengths are displayed in Fig. 2(a). In the absence of impurity ($V_s = 0$), the LDOS spectrum is V shaped with two peaks at the energies $\pm E_0$, as indicated in Fig. 2(a). When the point impurity is added, some additional low-energy states are induced by the impurity (indicated by the arrow), with the energies depending on the impurity strength V_s . As the impurity strength is weak ($V_s = 5$), the additional state appears at the negative energy. When the strength increases to $V_s = 10$, a sharp resonant peak appears near the zero energy. As V_s increases to 15, the peak shifts to the positive energy and the peak intensity decreases rapidly. As V_s increases further, only a broad hump feature exists at a saturating positive energy. Our numerical results indicate that for a bulk impurity in the NLS system, the impurity states exist for all of the impurity strengths we considered. However, the impurity resonant state, behaving as a sharp low-energy peak,

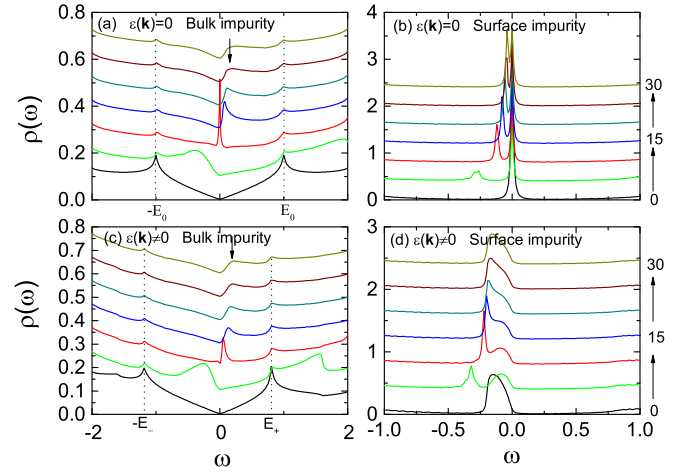


FIG. 2. The LDOS spectra near a bulk impurity and surface impurity with $\varepsilon(\mathbf{k}) = 0$ and $\varepsilon(\mathbf{k}) \neq 0$, respectively. From bottom to top, the impurity strengths (V_s) are 0, 5, 10, 15, 20, 25, and 30, respectively.

is not robust and exists only for a very small parametric range of the impurity strength.

We move to study the surface impurity effects. The LDOS spectra near a surface impurity [at the site (0, 1) in the $y = 1$ plane] are plotted in Fig. 2(b). As the impurity strength is zero, there is a sharp peak at the zero energy, due to the surface states from the zero-energy flat band. In the presence of the point impurity, an additional peak appears, with the energy moving towards the zero energy as V_s increases. One can see that the effect of a surface impurity is significantly different from that of a bulk one. Here, the impurity-induced sharp resonant peak is robust and exists below the Fermi energy for all values of the positive impurity strengths we considered.

Now let us study the impurity effects with chiral symmetry breaking, i.e., $\varepsilon(\mathbf{k}) \neq 0$. The corresponding numerical results of the LDOS spectra are presented in Figs. 2(c) and 2(d). Note that the bare LDOS spectrum ($V_s = 0$) is asymmetric about zero energy ($E_- \neq E_+$), as seen in Fig. 2(c), consistent with the band spectrum shown in Fig. 1(b) [59]. For the bulk LDOS spectra, the impurity effects remain qualitatively the same, i.e., in the presence of an impurity term, there are some low-energy features, with the energy shifting from negative to positive when the impurity strengths become stronger. An impurity-induced resonant peak appears near the zero energy for a typical strength $V_s = 10$. For the surface spectra, in the absence of impurity, the low-energy peak becomes wider, due to the dispersion of the surface band. The peak width (about 0.2) is consistent with the width of the surface bandwidth shown in Fig. 1(b). In the presence of impurity, an additional resonant peak appears at the negative energy and approaches to the Fermi energy when the impurity strength increases. For rather strong strengths ($V_s \geq 20$), the impurity-induced resonant peak merges into the surface spectra and disappears. The impurity effects for $\varepsilon(\mathbf{k}) \neq 0$ are qualitatively similar to those for $\varepsilon(\mathbf{k}) = 0$, where the resonant peak induced by the surface impurity appears for a rather wide parametric range of impurity strengths and may be probed by the STM experiments.

The existence of the bound states induced by the impurity can usually be understood through analyzing the denominator of the T -matrix term $[A(\omega)]$ [39]. Here the complex function $A(\omega)$ is expressed as

$$A(\omega) = |\hat{I} - \hat{U} \hat{G}_0(\omega)|. \quad (10)$$

The resonant states appear when the pole condition $[A(\omega) \approx 0]$ satisfies. Generally for the fully gapped system, its imaginary part $[\text{Im}A(\omega)]$ should tend to zero when the energy is smaller than the system gap. Then a resonance would occur if its real part $[\text{Re}A(\omega)]$ also equals to zero at a certain energy level. For the nodal system, $\text{Im}A(\omega)$ is usually finite and only tends to zero near the band crossing energy, where the resonance may occur. Here, the bulk energy bands are not fully gapped and a nodal line exists. The resonant condition is difficult to achieve except for very low energies around the nodal line with vanishing DOS. In contrast, for the case of a surface impurity, the weight of the bare LDOS is dominated by the surface states and centers at the zero energy. The LDOS spectra away from the zero energy are suppressed greatly, so that the imaginary part $\text{Im}A(\omega)$ is rather small in a large energy scale, similar to gapped systems. As a result, resonant states may appear if the pole condition holds at this energy scale. The above qualitative analysis partly explains our numerical results. We plot the real and imaginary parts of the function $A(\omega)$ [obtained from Eq. (10)] in Fig. 3 to investigate and display in more detail the mechanism of the resonant states. For the bulk impurity with $V_s = 10$, as seen in Figs. 3(a) and 3(b), a pole occurs near the zero energy at the frequency ω_p when $\text{Re}A(\omega)$ equals to zero. At the same time, $\text{Im}A(\omega)$ approaches zero near the Fermi energy, and then a resonant behavior occurs. For the surface impurity, as seen in Figs. 3(c) and 3(d), the pole condition can also be satisfied for this impurity strength, leading to the resonant impurity states [59].

For the surface impurity effect, the impurity-induced bound state is rather robust as we presented above. Generally for such robust resonant peak there may exist some nontrivial mechanism. Thus we would like to discuss this issue in more

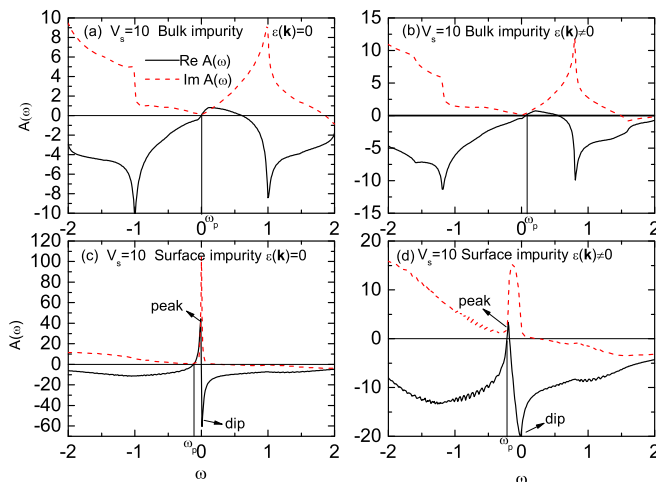


FIG. 3. The real and imaginary parts of $A(\omega)$ as a function of the frequency ω .

detail to get a deeper understanding for this resonant state. For a surface impurity, there are two non-zero elements for the \hat{U} matrix, namely, $U_{11} = U_{22} = V_s$. To obtain a qualitative understanding of the mechanism, we neglect the off-diagonal Green's function and rewrite the complex function $A(\omega)$ approximately as

$$A(\omega) \approx [1 - V_s G_{011}(\omega)][1 - V_s G_{022}(\omega)]. \quad (11)$$

Then the imaginary part of $A(\omega)$ is obtained as

$$\text{Im}A(\omega) \approx -V_s \sum_{i=1}^2 \text{Im}G_{0ii}(\omega). \quad (12)$$

On the system surface, due to the zero-energy flat band, most spectral weight concentrates to the zero energy. $\text{Im}A(\omega)$ is rather small at the nonzero energy and a sharp peak develops at the zero energy.

Now let us analyze the real part of $A(\omega)$ $[\text{Re}A(\omega)]$. For an impurity with a strong scattering strength, when the energy is far away from the zero energy, we have $V_s G_{0ii}(\omega) \gg 1$. $\text{Re}A(\omega)$ can be expressed approximately as

$$\begin{aligned} \text{Re}A(\omega) \approx & V_s^2 \text{Re}G_{011}(\omega) \text{Re}G_{022}(\omega) \\ & - V_s^2 \text{Im}G_{011}(\omega) \text{Im}G_{022}(\omega). \end{aligned} \quad (13)$$

Then we have $\text{Re}A(\omega) \approx \text{Re}A(-\omega)$ from the spin-flipped particle-hole symmetry [59].

When the energy approaches to zero, the properties of $\text{Re}A(\omega)$ can be obtained from $\text{Im}A(\omega)$. $\text{Im}A(\omega)$ changes suddenly at the two sides of the zero-energy peak, leading to a pair of logarithmic singularities in $\text{Re}A(\omega)$ via the Kramers-Kronig relation [60]. In actual calculations, these two singularities lead to $\text{Re}A(\omega)$ exhibiting a sharp peak at the slightly negative energy, and a sharp dip at the slightly positive energy, as indicated in Fig. 3(c). Note that the pair of singularities will definitely lead to the pole condition being satisfied, namely, as the energy increases, at the negative energy, $\text{Re}A(\omega)$ increases from its normal value to nearly infinity. At the positive energy, $\text{Re}A(\omega)$ increases from nearly negative infinity to its normal value. And its normal value should be nearly symmetric with the zero energy $[\text{Re}A(\omega) \approx \text{Re}A(-\omega)]$. As a result, $\text{Re}A(\omega)$ will definitely cross the $y = 0$ axis at certain low energy. Therefore, here the pole condition will generally be satisfied for a strong impurity strength. For the present energy band, $\text{Re}A(\omega)$ is negative when the energy is away from the Fermi energy, as presented in Fig. 3(c). Then the peaklike singularity at negative energy leads to the pole condition being generally satisfied at certain negative energy.

For the case of $\varepsilon(\mathbf{k}) \neq 0$, the surface band has a dispersion. Therefore, $\text{Re}A(\omega)$ has no strict singularity. While a peak at the negative energy and a dip at the positive energy still exist, as indicated in Fig. 3(d). These peak and dip structures will lead to the pole condition being satisfied for a wide parametric range.

The origin and mechanism of the resonant state induced by a surface impurity is rather special. They are different from any kind of impurity-induced bound states proposed previously for other systems [39,41–56]. It does indeed arise from a surface flat band. Rather interestingly, this mechanism is analogous to that of the (π, π) spin resonance in high- T_c superconductors [61,62].

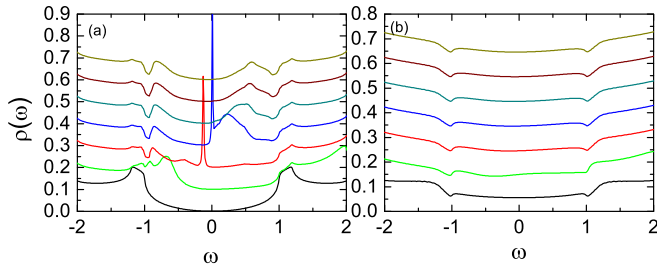


FIG. 4. The LDOS spectra for the Weyl semimetal. (a) The LDOS spectra near a bulk impurity. (b) The LDOS spectra near a surface impurity. From bottom to top, the impurity strengths (V_s) are 0, 5, 10, 15, 20, 25, and 30, respectively.

We have clarified that the flat band at the system surface should play the essential role to generate the bound state. The surface flat bands are protected by the bulk band topology under the \mathcal{PT} symmetry [4]. The impurity term [Eq. (2)] obeys the \mathcal{PT} symmetry and does not change the topological properties of the system. Therefore, the resonant states induced by the surface impurity is robust and exist for a wide parametric range of impurity strengths. We expect that such a resonant peak can be observed in experiments which may provide a clear signature to probe the topological surface states in NLS materials.

It is worthwhile to investigate the impurity effects in the Weyl semimetal, and compare it with that for the topological NLS. A minimal lattice model to describe the topological NLS can be obtained by adding the term $\sum_{\mathbf{k}} 2\lambda_0 \sin k_x \sigma_1$ to Eq. (1) [$\varepsilon(\mathbf{k}) = 0$ is adopted in the calculation]. Then, two point nodes $(0, 0, \pm\pi/2)$ are obtained with the present parameters. At the system surface, a Fermi arc connecting the two nodal points can be obtained.

The impurity effects for the Weyl semimetal are studied in Fig. 4. The LDOS spectra at the nearest neighbor of a bulk and a surface impurity are plotted in Figs. 4(a) and 4(b), respectively. As seen in Fig. 4(a), for the bulk impurity, the bound states seem to be qualitatively similar to those in NLSs, namely, a sharp resonance peak appears at near zero energy for certain impurity strength. When the impurity strength is

rather weak or strong, only a low-energy hump exists. Note that here the resonant states can survive for a relatively wider range of strength, compared with the bulk impurity effects of NLSs. On the other hand, for the surface impurity, the results for Weyl semimetals are significantly different from those for NLSs. As seen in Fig. 4(b), there are no visible impurity-induced low-energy features for all of the strengths we considered. Unlike the zero-energy peak of the bare LDOS in the NLS, the Fermi arc surface states distribute in a finite energy scale and lead to a nearly constant LDOS. As a result, the resonant states cannot form. We also compare the results of three-dimensional topological insulators. It was reported that robust bound states can be induced by a bulk impurity [53–55], while the impurity bound states cannot form at the system surface [54]. From the discussion above, one can see that the existence of a sharp impurity resonant peak at the system surface can serve as a notable feature for topological NLSs and may be used to distinguish the NLSs from some of the other topologically nontrivial materials experimentally.

IV. SUMMARY

In summary, single impurity effects in nodal-line semimetals have been systematically studied based on the T -matrix method. For a bulk impurity, there are some low-energy features for all of the impurity strengths we considered, while the impurity resonant states exist only near the Fermi energy for a certain range of impurity strength. For the surface impurity, there is a resonant impurity state for a rather wide parametric range of impurity strength. We also compare our results with those in other three-dimensional topologically nontrivial materials and conclude that the existence of the robust resonant impurity state at the system surface may provide a useful probe for the topological surface states in nodal-line semimetals.

ACKNOWLEDGMENTS

This work was supported by the NKRDP of China (Grant No. 2016YFA0301800), the GRF (Grants No. HKU 173309/16P and No. HKU173057/17P), and the CRF (Grant No. C6005-17G) of Hong Kong.

-
- [1] A. A. Burkov, M. D. Hook, and L. Balents, Topological nodal semimetals, *Phys. Rev. B* **84**, 235126 (2011).
- [2] Y. Kim, B. J. Wieder, C. L. Kane, and A. M. Rappe, Dirac Line Nodes in Inversion-Symmetric Crystals, *Phys. Rev. Lett.* **115**, 036806 (2015).
- [3] R. Yu, H. Weng, Z. Fang, X. Dai, and X. Hu, Topological Node-Line Semimetal and Dirac Semimetal State in Antiperovskite Cu_3PdN , *Phys. Rev. Lett.* **115**, 036807 (2015).
- [4] D.-W. Zhang, Y. X. Zhao, R.-B. Liu, Z.-Y. Xue, S.-L. Zhu, and Z. D. Wang, *Phys. Rev. A* **93**, 043617 (2016).
- [5] W. Chen and J. L. Lado, *Phys. Rev. Lett.* **122**, 016803 (2019).
- [6] J. Hu, Z. Tang, J. Liu, X. Liu, Y. Zhu, D. Graf, K. Myhro, S. Tran, C. N. Lau, J. Wei, and Z. Mao, *Phys. Rev. Lett.* **117**, 016602 (2016).
- [7] J. Hu, Y. L. Zhu, D. Graf, Z. J. Tang, J. Y. Liu, and Z. Q. Mao, *Phys. Rev. B* **95**, 205134 (2017).
- [8] N. Kumar, K. Manna, Y. Qi, S.-C. Wu, L. Wang, B. Yan, C. Felser, and C. Shekhar, *Phys. Rev. B* **95**, 121109(R) (2017).
- [9] H. Pan, B. Tong, J. Yu, J. Wang, D. Fu, S. Zhang, B. Wu, X. Wan, C. Zhang, X. Wang, and F. Song, *Sci. Rep.* **8**, 9340 (2018).
- [10] W. Chen, K. Luo, L. Li, and O. Zilberberg, *Phys. Rev. Lett.* **121**, 166802 (2018).
- [11] W. Chen, H.-Z. Lu, and O. Zilberberg, *Phys. Rev. Lett.* **122**, 196603 (2019).
- [12] R. Li, H. Ma, X. Cheng, S. Wang, D. Li, Z. Zhang, Y. Li, and X.-Q. Chen, *Phys. Rev. Lett.* **117**, 096401 (2016).

- [13] Y. Huh, E.-G. Moon, and Y. B. Kim, *Phys. Rev. B* **93**, 035138 (2016).
- [14] B. Roy, *Phys. Rev. B* **96**, 041113(R) (2017).
- [15] G. E. Volovik, *J. Supercond. Novel Magn.* **26**, 2887 (2013).
- [16] M. Hirayama, R. Okugawa, T. Miyake, and S. Murakami, *Nat. Commun.* **8**, 14022 (2017).
- [17] A. Lau and C. Ortix, *Phys. Rev. Lett.* **122**, 186801 (2019).
- [18] D. Takane, Z. Wang, S. Souma, K. Nakayama, C. X. Trang, T. Sato, T. Takahashi, and Y. Ando, *Phys. Rev. B* **94**, 121108(R) (2016).
- [19] A. Topp, J. M. Lippmann, A. Varykhalov, V. Duppel, B. V. Lotsch, C. R. Ast, and L. M. Schoop, *New J. Phys.* **18**, 125014 (2016).
- [20] M. Neupane, I. Belopolski, M. M. Hosen, D. S. Sanchez, R. Sankar, M. Szlawaska, S.-Y. Xu, K. Dimitri, N. Dhakal, P. Maldonado, P. M. Oppeneer, D. Kaczorowski, F. Chou, M. Z. Hasan, and T. Durakiewicz, *Phys. Rev. B* **93**, 201104(R) (2016).
- [21] L. M. Schoop, M. N. Ali, C. Straßer, A. Topp, A. Varykhalov, D. Marchenko, V. Duppel, S. S. P. Parkin, B. V. Lotsch, and C. R. Ast, *Nat. Commun.* **7**, 11696 (2016).
- [22] M. M. Hosen, K. Dimitri, A. Aperis, P. Maldonado, I. Belopolski, G. Dhakal, F. Kabir, C. Sims, M. Z. Hasan, D. Kaczorowski, T. Durakiewicz, P. M. Oppeneer, and M. Neupane, *Phys. Rev. B* **97**, 121103(R) (2018).
- [23] M. Mofazzel Hosen, G. Dhakal, K. Dimitri, P. Maldonado, A. Aperis, F. Kabir, C. Sims, P. Riseborough, P. M. Oppeneer, D. Kaczorowski, T. Durakiewicz, and M. Neupane, *Sci. Rep.* **8**, 13283 (2018).
- [24] G. Bian, T.-R. Chang, R. Sankar, S.-Y. Xu, H. Zheng, T. Neupert, C.-K. Chiu, S.-M. Huang, G. Chang, I. Belopolski, D. S. Sanchez, M. Neupane, N. Alidoust, C. Liu, B. Wang, C.-C. Lee, H.-T. Jeng, C. Zhang, Z. Yuan, S. Jia, A. Bansil, F. Chou, H. Lin, and M. Z. Hasan, *Nat. Commun.* **7**, 10556 (2016).
- [25] X. Xu, Z. Kang, T.-R. Chang, H. Lin, G. Bian, Z. Yuan, Z. Qu, J. Zhang, and S. Jia, *Phys. Rev. B* **99**, 104516 (2019).
- [26] Q. Xu, R. Yu, Z. Fang, X. Dai, and H. Weng, *Phys. Rev. B* **95**, 045136 (2017).
- [27] Y. Quan, Z. P. Yin, and W. E. Pickett, *Phys. Rev. Lett.* **118**, 176402 (2017).
- [28] Y. Wu, L.-L. Wang, E. Mun, D. D. Johnson, D. Mou, L. Huang, Y. Lee, S. L. Bud'ko, P. C. Canfield, and A. Kaminski, *Nat. Phys.* **12**, 667 (2016).
- [29] T. Sato, Z. Wang, K. Nakayama, S. Souma, D. Takane, Y. Nakata, H. Iwasawa, C. Cacho, T. Kim, T. Takahashi, and Y. Ando, *Phys. Rev. B* **98**, 121111(R) (2018).
- [30] D. Takane, S. Souma, K. Nakayama, T. Nakamura, H. Oinuma, K. Hori, K. Horiba, H. Kumigashira, N. Kimura, T. Takahashi, and T. Sato, *Phys. Rev. B* **98**, 041105(R) (2018).
- [31] L. S. Xie, L. M. Schoop, E. M. Seibel, Q. D. Gibson, W. Xie, and R. J. Cava, *APL Mater.* **3**, 083602 (2015).
- [32] Y. H. Chan, C. K. Chiu, M. Y. Chou, and A. P. Schnyder, *Phys. Rev. B* **93**, 205132 (2016).
- [33] B. Song, C. He, S. Niu, L. Zhang, Z. Ren, X.-J. Liu, and G.-B. Jo, *Nat. Phys.* **15**, 911 (2019).
- [34] D. W. Zhang, Y. Q. Zhu, Y. X. Zhao, H. Yan, and S. L. Zhu, *Adv. Phys.* **67**, 253 (2019).
- [35] T. Bzdušek, Q. Wu, A. Rüegg, M. Sigrist, and A. A. Soluyanov, *Nature (London)* **538**, 75 (2016).
- [36] W. Chen, H.-Z. Lu, and J.-M. Hou, *Phys. Rev. B* **96**, 041102(R) (2017).
- [37] Z. Yan, R. Bi, H. Shen, L. Lu, S.-C. Zhang, and Z. Wang, *Phys. Rev. B* **96**, 041103(R) (2017).
- [38] M. Ezawa, *Phys. Rev. B* **96**, 041202(R) (2017).
- [39] A. V. Balatsky, I. Vekhter, and J.-X. Zhu, *Rev. Mod. Phys.* **78**, 373 (2006).
- [40] Ø. Fischer, M. Kugler, I. Maggio-Aprile, C. Berthod, and C. Renner, *Rev. Mod. Phys.* **79**, 353 (2007).
- [41] W.-F. Tsai, Y.-Y. Zhang, C. Fang, and J. Hu, *Phys. Rev. B* **80**, 064513 (2009).
- [42] T. Zhou, H. Huang, Y. Gao, J.-X. Zhu, and C. S. Ting, *Phys. Rev. B* **83**, 214502 (2011).
- [43] O. A. Awoga and A. M. Black-Schaffer, *Phys. Rev. B* **97**, 214515 (2018).
- [44] J. D. Sau and E. Demler, *Phys. Rev. B* **88**, 205402 (2013).
- [45] X.-J. Liu, *Phys. Rev. A* **87**, 013622 (2013).
- [46] Y. Nagai, Y. Ota, and M. Machida, *J. Phys. Soc. Jpn.* **84**, 034711 (2015).
- [47] M. Wimmer, A. R. Akhmerov, M. V. Medvedyeva, J. Tworzydło, and C. W. J. Beenakker, *Phys. Rev. Lett.* **105**, 046803 (2010).
- [48] H. Hu, L. Jiang, H. Pu, Y. Chen, and X.-J. Liu, *Phys. Rev. Lett.* **110**, 020401 (2013).
- [49] Y. Nagai, Y. Ota, and M. Machida, *Phys. Rev. B* **89**, 214506 (2014).
- [50] Y. Nagai, Y. Ota, and M. Machida, *J. Phys. Soc. Jpn.* **83**, 094722 (2014).
- [51] T. Zhou, Y. Gao, and Z. D. Wang, *Phys. Rev. B* **98**, 024515 (2018).
- [52] C. Setty, P. W. Phillips, and A. Narayan, *Phys. Rev. B* **95**, 140202(R) (2017).
- [53] R. R. Biswas and A. V. Balatsky, *Phys. Rev. B* **81**, 233405 (2010).
- [54] J. Lu, W.-Y. Shan, H.-Z. Lu, and S.-Q. Shen, *New J. Phys.* **13**, 103016 (2011).
- [55] R.-J. Slager, L. Rademaker, J. Zaanen, and L. Balents, *Phys. Rev. B* **92**, 085126 (2015).
- [56] Z. Huang, T. Das, A. V. Balatsky, and D. P. Arovas, *Phys. Rev. B* **87**, 155123 (2013).
- [57] P. Hirschfeld, D. Vollhardt, and P. Wölfle, *Solid State Commun.* **59**, 111 (1986).
- [58] S. Schmitt-Rink, K. Miyake, and C. M. Varma, *Phys. Rev. Lett.* **57**, 2575 (1986).
- [59] See Supplemental Material at <http://link.aps.org/supplemental/10.1103/PhysRevB.100.205119> for the spin-flipped particle-hole transformation and spin-dependent bare Green's function.
- [60] B. Yu-Kuang Hu, *Am. J. Phys.* **57**, 821 (1989).
- [61] J. Brinckmann and P. A. Lee, *Phys. Rev. Lett.* **82**, 2915 (1999).
- [62] J.-X. Li, C.-Y. Mou, and T. K. Lee, *Phys. Rev. B* **62**, 640 (2000).